

## Engineering joint seismic monitoring with sparse networks: progress toward providing seismic information to operators

Paul A. Nyffenegger<sup>1</sup>, K. D. Hutchenson<sup>1</sup>, Brendan Kolkman-Quinn<sup>3</sup>, D. Quigley<sup>1</sup>, Elige B. Grant<sup>1</sup>, J. Yelton<sup>1</sup>, Mike Dahl<sup>2</sup>, Marie Macquet<sup>3</sup>

<sup>1</sup>Geospace Technologies, <sup>2</sup>Geospace Technologies, Ca.

<sup>3</sup>Carbon Management Canada

### Summary

Geospace installed a sparse network of four permanent compact volumetric phased SADAR arrays at Carbon Management Canada's Newell County Field Research Station (FRS) outside Brooks, Alberta, Canada, in the Fall of 2021 for microseismic monitoring of the FRS geological carbon sequestration (GCS) technology proving ground. The SADAR arrays have also been demonstrated to supply active-source survey imaging capabilities for generating optimum offset seismic profiles. The sparse network design is expandable with the growth of the plume and will be able to take advantage of permanent sources outside the VSP imaging range for on demand active-source spot/patch imaging.

The joint active and passive combined capabilities of sparse networks of SADAR arrays offer both sets of information from one set of instrumentation to facility engineers responsible for sustaining ongoing operations and managing geologic assets. Integrating the active-source seismic imaging functions with the SADAR network passive monitoring infrastructure allows for frequent conformance and containment verification at GCS projects, potentially providing facility engineers with an early warning of containment or conformance anomalies.

However, the processing and information management aspects of the joint functions will also require a total systems engineering approach to ensure the hardware systems, processing systems, and information systems are effectively integrated into monitoring and control systems typically present in modern industrial facilities. How best to engineer the information systems and fuse the joint seismic information is an ongoing effort. The integrated seismic monitoring capabilities of the SADAR array sparse network will provide facility engineers with improved information for understanding of the physical state of geologic assets and is applicable to mining, geothermal, SAG-D and EOR production, gas storage, and waste sequestration projects.

### Introduction

Configured as a sparse local network, four (4) SADAR compact volumetric phased arrays were deployed at the Carbon Management Canada (CMC) Field Research Station (FRS) in 2021 to provide persistent microseismic monitoring for ongoing geologic carbon sequestration (GCS) testing and evaluation (Nyffenegger et al., 2025a; Nyffenegger et al., 2023; Zhang et al., 2023; Hutchenson et al., 2023). The CMC-FRS additional monitoring equipment includes a network of 28 surface seismic stations in post holes, a permanent downhole network of 24 geophones,

distributed acoustic fiber sensor runs, 6 broadband seismometers, and various chemical, gravity, and other technologies monitoring the carbon dioxide injections into the ~300m depth Basal Belly River Sandstone (BRRS) (Lawton et al., 2019; Macquet et al., 2022). The sparse network of SADAR arrays includes the sensing, data acquisition, and data logging and storage functions on site, with the processing and analysis functions handled offsite. The system has been operating since installation at a 99% availability (Hutchenson et al., 2025b).

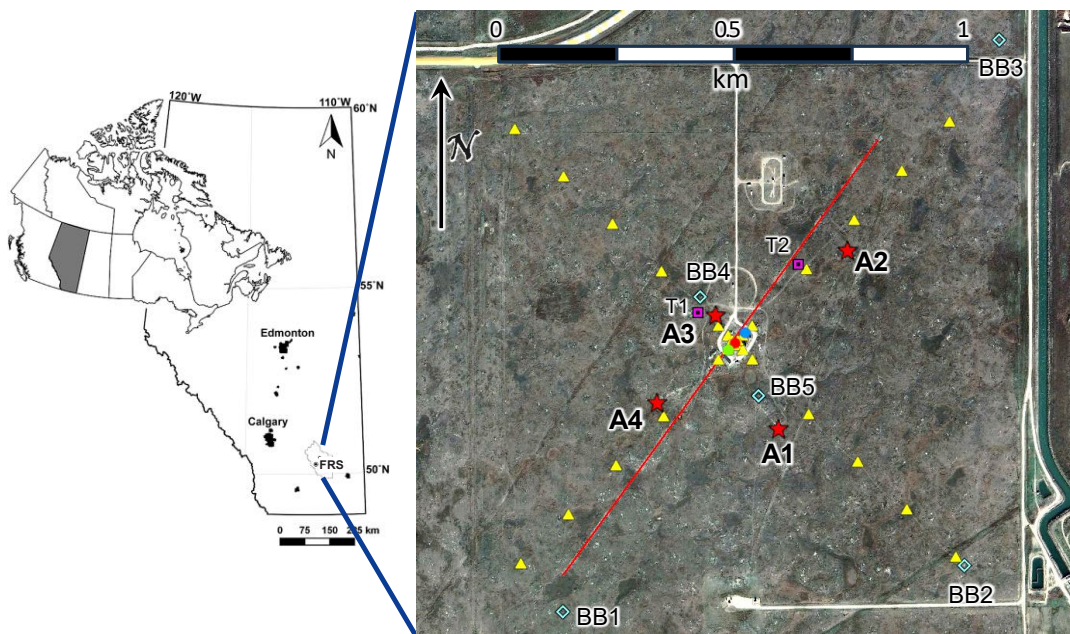


Figure 1. Location of the Carbon Management Canada Newell County Field Research Station, Alberta, Canada. The zoomed view indicates the injection well (red circle) and the four SADAR arrays (stars), 28 surface geophones (yellow triangles), the green circle marks the geophysical monitoring well with 24 borehole geophones, and BB labels are the broadband stations. SADAR array A3 is 70 m northwest of the injection well, A1 and A4 are 200 m from the injection well, and A2 is 300 m northeast of the well.

SADAR arrays are passive phased arrays, providing signal processing gains, siting flexibility, reduced footprints, a lower lifetime cost, and long-term risk reduction for measurement, monitoring, and verification (MMV) (Nyffenegger et al, 2025b, Nyffenegger et al., 2022). Three different volumetric phased array designs having 51 to 72 elements per array were installed at the FRS for testing and evaluation, and for developing systems engineering best practices for local permanent and continuous microseismic monitoring networks (Zhang et al, 2022, 2023). The array elements are vertical 10 Hz geophone sensors permanently installed in shallow boreholes at depths 9-21 m and then backfilled with a grout of bentonite and cement. The phased array designs have been sufficient to provide signal-to-noise ratio (SNR) gains required to detect and locate events with magnitudes as low as approximately -3 Mw.

While initially designed for passive microseismic monitoring, the SADAR arrays have demonstrated excellent capabilities for active source imaging (Quigley et al., 2025a; 2025b). The arrays furnish fixed position sensors for easily repeatable surveys supplying data with reduced noise levels and scattering distortion, and recording seismic surveys as a matter of regular daily operations. Current survey results from the FRS demonstrate optimum offset profiles resolving the shallow BBRS reservoir, the Manneville, and the Basal Cambrian sands that overlay crystalline basement, leveraging the existing microseismic monitoring capital investment (Hunter and Pullan, 1989; Lawton et al., 2022; Nyffenegger et al., 2025b). Moreover, the infrastructure and processing are in place for time-lapse analysis of the optimum offset images.

Historically, seismic phased arrays were first deployed for global nuclear monitoring more than a half-century ago (Douglas, 2013). Because the global and regional monitoring arrays were all designed for frequencies below 10 Hz, planar designs were the only practical alternatives for maximizing array aperture given the large wavelengths while being limited by overall coherence lengths. Today, applications requiring local volume monitoring and improvements in geophone sensor frequency response allow acquisition of substantially higher frequencies with shorter accompanying wavelengths, making compact volumetric designs for both microseismic monitoring and active source imaging practical and technically attractive (e.g., Hutchenson et al., 2025a; Lawton et al., 2022). Quantum/Geospace has been deploying SADAR compact volumetric arrays for about a decade for a variety of applications such as GCS facilities focusing on supplying derived information to engineers and operators (Zhang et al., 2022). For example, SADAR arrays have also been successfully deployed to monitor longwall coal mining at ~400 m depth and reservoir engineering activities deeper than 3 km.

In the case of the longwall coal mining demonstration, portable planar SADAR arrays were used in a network that progressed with the advance of the ~350m longwall face. The network comprised nine total phased arrays, arranged as two arrays interior of an irregular heptagon whose overall geometry would change as arrays were repositioned. The footprint of an individual array averaged ~300 m<sup>2</sup>; the total area covered by the network was ~1½ km<sup>2</sup>. For the reservoir engineering and monitoring demonstration, six total arrays were permanently deployed in a sparse network for a persistent and continuing reservoir monitoring during and after reservoir fracturing of nine ~3 km long horizontal wells. The network completely surrounds the horizontal wells; the field is ~4.5 km<sup>2</sup>. The volumetric design allows for a reduced footprint of ~50 m<sup>2</sup> per array; the total area covered by the network was ~24 km<sup>2</sup>. In both cases, the phased array and the network designs were engineered to meet requirements of providing the passive seismic information the engineers/operators were most concerned with, delivered as a periodic microseismic bulletin. The bulletin information is comprised of the continuous records of event locations, seismicity rates, moment magnitudes, moment as a function of time, other information derived from the waveforms, and spatial or volumetric expressions of these quantities. Reservoir engineering, underground mining, geothermal energy extraction, gas and GCS, heavy oil sands and EOR production, and reservoir engineering all benefit from the seismic information present in continuous seismicity catalogs.

The passive monitoring routine bulletin can be delivered to the operations engineers on a schedule or on demand. The latency tolerance for reporting “notifiable” events to field/facility operators is one of the key requirements driving total system engineering and affects overall costs. For example, emerging event clusters and changes in seismicity rates can be identified and reported periodically or upon exceeding a threshold condition. High interest events, for example those surpassing a magnitude threshold or within a pre-identified geologic volume, will be reported as soon as possible, limited by connectivity to networks. When deployments require near-real-time reporting with guaranteed near 100% availability, wired networked solutions generally become more cost-effective than redundant wireless connectivity with independent power sources. As these latency and availability requirements are relaxed, other solutions become possible that may result in lower overall capital or reoccurring costs.

In comparison, generating images from the sparse network happens on a survey-by-survey basis, triggered by completion of a standard, patch, or VSP survey and transfer of the necessary inputs to the processing system. In these cases, image generation will need to be automated to reduce resulting image latencies, requiring automating the input of the survey technical information, timing, plan, etc., best accomplished with automated position and action logging of the source. The current, largely-manual processing methods demonstrated using the sparse SADAR network and regular VSP surveys at the FRS may be automated at least through image generation. Automation of time-lapse image analysis is an ongoing effort. In contrast, analysis of records associated with automated permanent source shots that are remotely triggered according to a schedule is relatively straight forward; a semi-automated workflow using the FRS test cases has already been developed (Lawton et al., 2022; Kolkman-Quinn et al., 2024; Nyffenegger et al., 2025b).

Providing operations engineers with fused seismic information from the continuous seismicity catalog and the optimum offset images, both supplied from a single sparse network permanent and persistent acquisition system, is an ongoing development effort. However, the individual seismic monitoring functions using the sparse network are beyond proof-of-concept and developed to the point of joint or total systems engineering. This article outlines a potential systems engineering process, some of the considerations for planning the initial deployment, and a set of results for both passive monitoring and active source survey functions.

## Methods

Fielding a robust, efficient, and economical passive microseismic monitoring system that is reliable for the life of the field demands the rigor of a total systems engineering approach. The sensors, data acquisition chain, communications, data storage, and processing pipelines, must be considered as critical interrelated subsystems of the overall unified seismic monitoring system. Following a standard systems engineering approach, a successive hierarchy of requirements are broken down to functional components and tasks, the technical architectures and subsystems are defined, and the risks associated with each subsystem are identified, assessed, and mitigated where possible at the design phase. In addition, a total systems engineering approach ensures

the passive microseismic monitoring outputs are effectively integrated into the facility operations control systems, and that verification and validation, both for initial functionality and as a maintenance operation, are built into the combined system plan.

Engineering a joint passive monitoring and active source survey system requires integrating functions at the requirements level. Integration of the two seismic monitoring functions is difficult because the requirements for the different functions have led to very different preferred solutions for a) microseismic monitoring, requiring relatively few high quality geometries with permanent specialized instruments to determine high accuracy locations, and b) active source imaging, requiring a plurality of densely sampled geometries with an abundance of temporarily deployed geophones. The systems engineering approaches currently under construction address integrated seismic monitoring functions from a single system, focusing on what information the sparse network can provide to an operations control center. The information requirements of the control center become the priority, like in the development of supervisory control and data acquisition (SCADA) systems. SCADA systems and distributed control systems (DCS) are common in modern critical infrastructure, transportation, and manufacturing facilities.

SADAR arrays are engineered using standard phased array principles starting with the requirements for bandwidth, the design frequency, sensor response, expected received signal levels for sources at reservoir depth and distance, and array gain to overcome noise. Non-signal chain requirements include latency tolerance and reliability, and significant design tradeoffs exist related to optimizing installation and reducing costs. Phased array design is always a site-specific exercise, requiring understanding the tradeoffs between signal coherency limits, noise and clutter field correlation and directionality, and the array gain needed to maximize the SNR within the desired frequency band.

The design goal for SADAR phased arrays is to achieve the largest practical aperture bounded by the coherence length, using the noise correlation distance limited element spacing for the required design frequencies and bandwidth so that site noise and clutter signals can be effectively suppressed. Simultaneously, the array layout is optimized to minimize the environmental footprint of the surface installation while still meeting performance and reliability requirements. The primary system requirements at the network level are specified for the area of review as a proxy for the monitored volume, including the minimum magnitude locatable event and the magnitude of completeness as a function of location, while considering land use and accessibility restrictions, power and communications accessibility, and latency tolerance.

The overall sparse network design performance for location of microseismic events is predicted also based on systems engineering approaches coupled with physics based estimates of the source energy, measurement based geological/geophysical models, the measured environmental noise, and the signal losses and gains against noise originating with energy propagation and signal processing steps (Nyffenegger et al., 2023; Grant et al., 2025). The array and network designs are iteratively refined to ensure they meet the passive monitoring requirements for

magnitude of completeness and area of review, while maintaining robust performance over the operating life of the field, even under the risk of sensor or component attrition. This SADAR array and passive network systems engineering process is appropriate for any of the underground asset operations where passive seismic monitoring provides advantageous information.

The passive monitoring processing pipeline is primarily an automated data reduction software that develops the critical monitoring information derived from combining the array data and performing measurements both on single arrays and across the network. The resulting information is the locations of microseismic events, their signal and source characteristics, and the uncertainties on both. The data processing pipeline software and the storage functions hardware and software are also engineered such that growth in the area of review can be accommodated by expanding the network with additional SADAR arrays where additional coverage is needed without rewriting or recompiling the automated processing pipeline. The processing pipeline systems engineering leads to a scalable, modular, containerized software and information management system appropriate for controlling the overall cost of the seismic MMV functions. The processing pipelines' inputs consist of the phased array data, the arrays' configuration information, the geophysical and geological models, and signal and information processing function configuration information.

Standard phased array signal processing techniques such as beamforming and gradiometry are applied within the pipeline. Beamforming operations maximize the SNR of the received signal by suppressing incoherent noise and coherent clutter signals arriving along directions different from the beam main response axis (MRA). SNR improvements allow lower magnitude microseismic detections and improved phase onset estimates, as well as direct measurements of phase velocity and arrival angle. SNR enhancements and measured features also enable accurate phase association across the network leading to better microseismic locations with lower uncertainties. Beamforming discussion is continued in the active source survey processing methods below.

The automated pipelines for these microseismic monitoring systems are engineered to apply detection methods simultaneously across a suite of beams covering a planned MRA geometry, processed in near real time if supported by communications and power infrastructure. Detection association, location, and source parameter estimation such as moment magnitude complete the automated pipeline, followed by analyst review of the resulting bulletin (e.g. Zhang et al 2023). The processing pipeline outputs consist of the microseismic event catalog as represented in the system information model and relational database, and the condensed bulletin summarizing that information based on the operators priorities. The catalog information is stored in the system's relational database, along with metrics derived from the raw data indicative of data quality and array/network state of health. Lastly, information useful for continuous monitoring of the facility is derived from the catalog as previously discussed, all served graphically to operators for determining that the state of the asset is stable and conforms to expectations, or that actions need to be taken.

An integrated, combined passive microseismic and active survey sparse network using phased array designs has not previously been engineered. The engineering requirements and design processes outlined here are a prototype for a total system engineering of the integrated seismic monitoring functions. A jointly designed integrated sparse network plan is expected to start with an optimized passive microseismic network and SADAR arrays as those requirements are expected to be more restrictive. A total systems engineering approach then would merge the seismic imaging requirements with the initial microseismic monitoring plan.

In general, it is expected that the early imaging of the reservoir response to injection operations will be performed using vertical seismic profiling (VSP). Semi-automated VSP acquisition can provide rapid time-lapse imaging during the initial stages of the injection to verify conformance and containment and provide early warning of anomalies (Pevzner et al., 2021). However, for commercial GCS operations injecting, for example, ~1 kiloton per day for a project lifetime exceeding many years, the plume is expected to quickly grow beyond the ability of VSP surveys to measure (e.g., Kolkman-Quinn et al., 2025) without drilling and instrumenting additional monitoring wells.

In contrast, extending the VSP constant azimuth survey lines can be used with a properly designed SADAR array network to image limited sections of the reservoir. The additional active-source imaging system requirements will focus primarily on network configuration and array placement rather than on the individual arrays, under the assumptions that the array gains required for the passive functions are sufficient for active source imaging. A primary objective is to design a sparse network that is complementary to the early VSP surveys and will extend the common coverage points between areas covered by the downhole receivers and the volumetric phased array network for extended VSP survey lines. Designing the arrays for microseismic monitoring with an upper design frequency between 150 Hz and 200 Hz will adequately cover the frequency band of greatest interest for both functions. The array designs required to produce SNR gains sufficient for detecting microseismic events with magnitudes below ~0 Mw generally have also been effective in the FRS surveys for beating down noise levels in active-source surveys and imaging strata down to the crystalline basement.

At the network level then, the specific imaging requirements are derived from regulatory and operational requirements levied on monitoring techniques to prove containment and conformance assessments, and to mitigate containment risks from unknown faults and fractures within a storage complex. The initial requirement is to identify volumes to be surveyed repeatedly by VSP and SADAR techniques and then adjust the planned microseismic network and survey designs to best meet requirements. For the identified volumes, the specular reflection source-array midpoints are required to lie within the optimum offsets from the arrays. Therefore, optimizing the joint plan entails identifying the optimum offset ranges and the inner noise cone ranges (as shown in Quigley et al., 2025a and 2025b) for the planned microseismic network and adjusting the array locations or rerouting the survey lines such that the required survey overlap midpoints falls within the identified optimum offset zones. The optimum offset techniques often benefit from a survey

line being offset from the SADAR arrays rather than the array located on or near a survey line and also may benefit from not using perfectly straight source lines, instead maximizing the segment length within the optimum offset from an array. Additional technical requirements at the network level, such as required resurvey and reporting intervals can be derived, for example, from gap analysis of Kolkman-Quinn et al. (2025c) or from risk analysis and management frameworks (c.f. summary review in Nyffenegger et al., 2025a).

After settling the initial joint plan, the microseismic monitoring performance prediction must be recomputed to ensure that requirements are still satisfied. Engineering design options for satisfying both requirement sets include adding additional monitoring SADAR arrays to expand the range from the injection well that is monitored using the integrated approach, modifying surveys to include additional source lines that will be repeated for time-lapse monitoring, adding permanent remotely operated sources for improved subsurface sampling (for example, in Kolkman-Quinn et al., 2025a), and potentially relaxing requirements for the area of review, microseismic magnitude of completeness, locatable event threshold magnitude, or overlapping subsurface coverage. The options that do not involve relaxing requirements generally come with scaled increased costs with a notable exception: increasing the number of arrays without requiring a greater coverage area. That option for providing additional active source survey area using the optimum offset technique then would trigger a redesign of the phased arrays for the microseismic monitoring function to a lower gain requirement usually realized using fewer array elements. In that case, the increase in infrastructure costs may be partially offset by a decrease in equipment for the arrays.

As the area of review grows and prior to the physical plume edge expanding beyond the network boundaries, the seismic survey area will need to be expanded with additional arrays to meet the monitoring requirements. The expansion of the integrated sparse seismic monitoring system will require similar engineering considerations for network, survey, and array designs to meet the expanded area of review requirements while containing costs.

A possible approach has been proposed in Kolkman-Quinn et al. (2025b) where plume evolution is monitored using additional permanent source pedestals to expand the monitoring network. The permanent sources are relatively light weight and of limited acceleration output, but they are coupled to a steel screw pile pedestal anchored in bedrock or at least well below the weathering layer. Operators can trigger the remotely operated permanent sources on a schedule or as needed from a control room (Nyffenegger et al., 2025b). As a CO<sub>2</sub> plume evolves, additional screw piles may be installed, and the sources dismantled from unneeded sites to be installed at the new sites (Kolkman-Quinn et al., 2025b). Nevertheless, as the network is expanded, performance estimates will need to be updated for both the microseismic monitoring and the optimum offset imaging/monitoring functions, and then the estimates evaluated against field data according to standard systems engineering principals.

The approach to processing the active source VSP surveys to produce optimum offset images largely follows common approaches for generating basic receiver gathers with the exception of the additional beamform processing step (Quigley et al., 2025a, Quigley et al., 2025b). Currently, this processing system is beyond proof of concept but remains a developmental software engineering process. Descriptions of the initial basic signal conditioning and data quality monitoring steps are skipped here although these types of operations will be required in every system. A basic sequence for processing of the monitor survey lines can be broken down as 1) obtain survey data from the continuously acquired and stored records per phased array according to the shot schedule; append records where necessary, 2) Cut shot record segments per array element, 3) Cross correlate with sweep, 4) Average repeated shots per shot point, 5) Combine array element data using beamforming for targeted depth points, 6) Sort beamformed traces into “common receiver gather” cross-section, 7) Normal moveout correction, data scaling, and other enhancements. This sequence produces a starting profile for applying additional signal processing for improving the image or extracting attributes.

The beamforming operation listed as step (5) may be greatly expanded. The most basic approach is to generate a single beam per array using a delay-and-sum approach executed in the time or frequency domain, per shot point; i.e. individual beams are formed to individual target depth points. Beamforming data from the arrays targets specular reflections from horizon depths arriving at the array at a specific angle to maximize the received signal SNR. One beam per shot point is output. This procedure has also worked for processing permanent source shots from the tests performed at the FRS in 2024. Other valid phased array processing techniques may include adaptive beamforming, space-time adaptive beamforming, and non-linear beamforming. Furthermore, techniques such as dynamic beam steering and composite beam formation may be applied.

The beamformed data are usually sorted into receiver gathers that reveal an optimum-offset window of clean reflections outside the noise cone (Hunter and Pullan, 1989; Lawton et al., 2022; Kolkman-Quinn et al., 2024; Quigley et al., 2025b). The images are inherently stable to array element attrition and small deviations in source positions (Quigley et al., 2025a), making the approach well suited for time-lapse analysis. After an analyst defines the configurations and parameters required for input, follow on image generation for repeated geometries is expected to be automated.

The total systems engineering approach outlined in this section is expected to result in decreased technical and operational risks for the seismic MMV functions. Decreased risks usually result in decreased long-term costs.

### **Current Results from Existing Demonstrations at the FRS**

The current SADAR sparse network at the FRS provides the opportunity to assess the engineering of the hardware and software components from a total systems perspective. The opportunity to deploy arrays to the FRS developed quickly, and some shortcuts had to be

accepted to meet schedules before weather conditions prevented regular operations for installation into shallow boreholes. This section reports the planning and execution results, and the ongoing performance evaluated against the planned system. The general array design process is reported and evaluated but individual array designs are not evaluated.

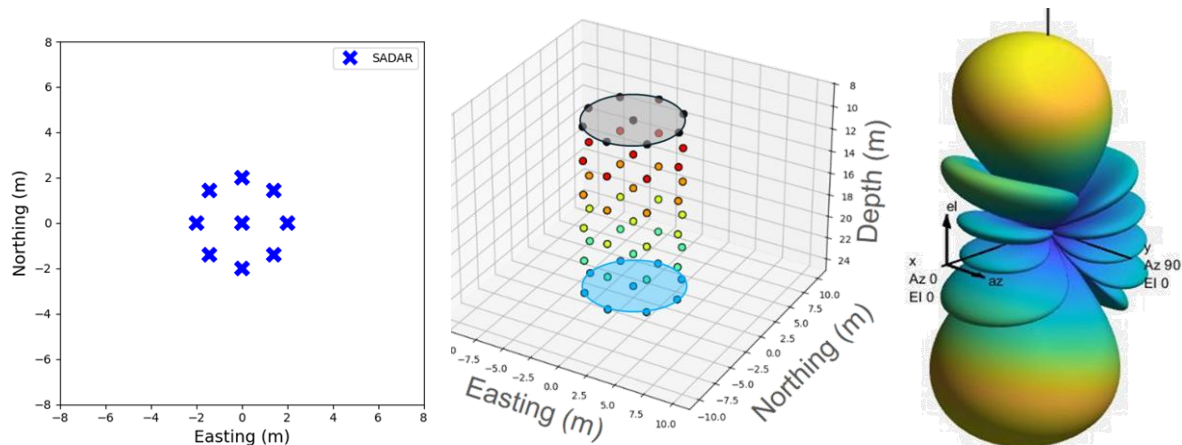


Figure 2. Array design “standard.” At left the octagonal array map view, and center in 3D profile view, and right array directivity index response pattern shown at the design frequency for a monochromatic incident plane wave at azimuth  $0^\circ$  and incident angle of  $160^\circ$  measured from vertical, aligned with the beam main response axis and a  $70^\circ$  depression angle (measured down from horizontal).

The array deployments were planned for a depth of  $\sim 10$  m for the top of the array depending on encountering any drilling difficulties so the entire array would be contained within the unconsolidated upper glacial deposits that reach  $\sim 30$  meters depth (Nyffenegger et al., 2022; Zhang et al., 2023, Hutchenson et al., 2025a). The array design parameters accepted against requirements previously listed were a) design frequency upper corner  $f_{dSc}=260$  Hz, b) desired frequency band of  $\sim 100$  Hz through 260 Hz (roughly 160 Hz), and c) compressional wave velocity  $v_d=800$  m/s, assumed based on measurements made in similar geologies. Although well logs exist for the FRS, we could not find measured velocities for these shallow depths within the schedule time allowance for design and planning. Without noise measurements available, a uniform cylindrical array (UCA) with a central column having octagonal element distribution becomes an attractive choice. The deficiencies in the inputs to the design process were acknowledged as risks and accepted, with the mitigation approach as modifying the design with additional elements (layers) and in the network design. The resulting *standard* design as shown in Figure 2 and labelled as A1 and A2 in Figure 1, uses  $N=54$  vertical geophone elements to supply a maximum gain against random noise of  $10 \cdot \log_{10}(N) \sim 17$  dB, not including any spatial filtering gains from beamforming. The directivity pattern of the *standard* array (Figure 2) illustrates the main beam and side lobes typical at the design frequency; refer to Zhang et al. (2023) for additional discussion on the array designs and directivity patterns.

The planned half-wavelength design element spacing for the *standard* array is  $\sim 1.5$  m (horizontally) with a circumscribed radius  $R \approx 2$  m. The vertical element spacing was chosen at 2m

to broaden out the band on the lower end corresponding to a design frequency for a vertical incident plane wave of  $f_{dS}=200$  Hz. Additional array designs were evaluated at the FRS based on similar input design parameters. A *wide aperture* version shown in Figure 3 installed at A3 in Figure 1 used nested UCAs, a total of 51 elements (17 boreholes by three levels), and two “horizontal” design frequencies  $f_{dWA1}=200$  Hz and  $f_{dWA2}=175$  Hz having a maximum circumscribed radius of 3.75 m, with the vertical element spacing the same as in the *standard*. A temporary multicomponent patch phased array (Figure 3) was later installed on the surface above A3 for comparisons with gain and noise levels having the same number of elements, multiple design frequencies extending lower than those for the volumetric arrays, and a total horizontal aperture of  $\sim 24$ m (about twice the aperture of the wide-aperture volumetric array) (Grant et al., 2025, Hutchenson et al., 2025b).

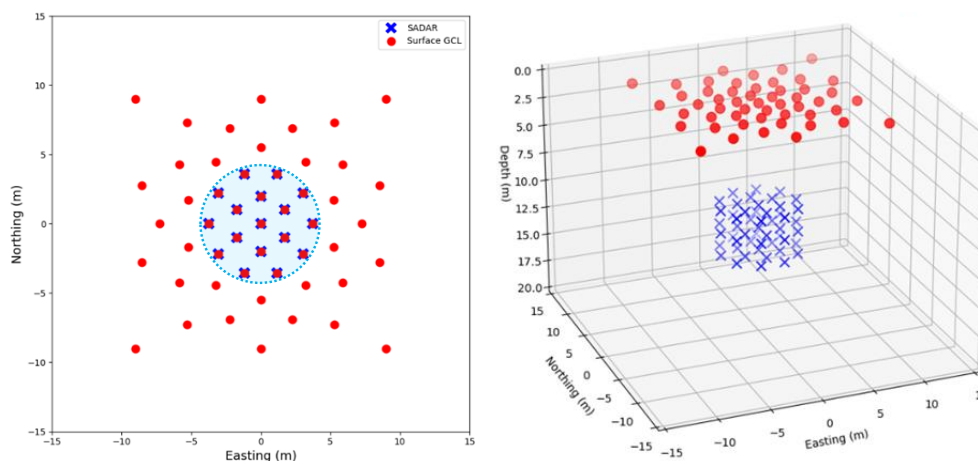


Figure 3. Array design “wide aperture.” At left, the wide aperture array and the temporary surface patch array in map view, with the footprint of the volumetric array shown as the cyan shaded circle. At right, both arrays are shown in 3D profile view.

Installation of the arrays has been discussed in Zhang et al. (2023), and Hutchinson et al. (2025a). The installation and activation of all four arrays was completed in seven days and was perhaps the best planned and executed portion of the ongoing project. The surveying, drilling of the boreholes, grouting, and emplacement of the sensor strings followed a systems engineering plan that included a logistics plan, construction and emplacement phase, connection phase, and functional testing and evaluation at the completion. In addition, all components were originally qualified at the factory. At the close out of the installation, the sensor, data acquisition systems, and connectivity and data logging systems were all verified as performing to specification.

Compressional phase velocity measurements taken directly from the arrays after installation indicate that the actual velocities are at least  $\sim 1$  km/sec and as high as  $\sim 1.8$  km/sec, substantially higher than what was assumed. The net effect of the velocity underestimation is a shift in the design frequency and bandwidth of the array response, i.e. the frequency band that the array maximizes SNR gains shifts to higher frequencies. At  $v_d=[1, 1.8]$  km/sec, the standard array upper

corner design frequency  $f_{dsc}=[330, 580]$  Hz and the bottom of the band climbs well above 100 Hz depending on incidence angle.

The measured array gain against random noise can be approximated using an “infinite velocity beam,” as shown in Figure 4 for both SADAR A3 and the surface patch array. However, this method underestimates gain due to directivity, i.e. the spatial filtering provided by beamforming. The gains against noise by depth of emplacement are demonstrated by comparing the single element measurements (dashed lines), and the array gain is estimated by comparing the dashed line with the solid line for the individual arrays. At frequencies above 100 Hz the SADAR array is performing as expected with gains approaching 20 dB. Below 100 Hz the gain decreases as wavelength increases and the noise on the individual elements becomes correlated, until there is almost no gain at 20 Hz. Furthermore, at the frequencies where the gain is lost the directivity pattern approaches omnidirectional.

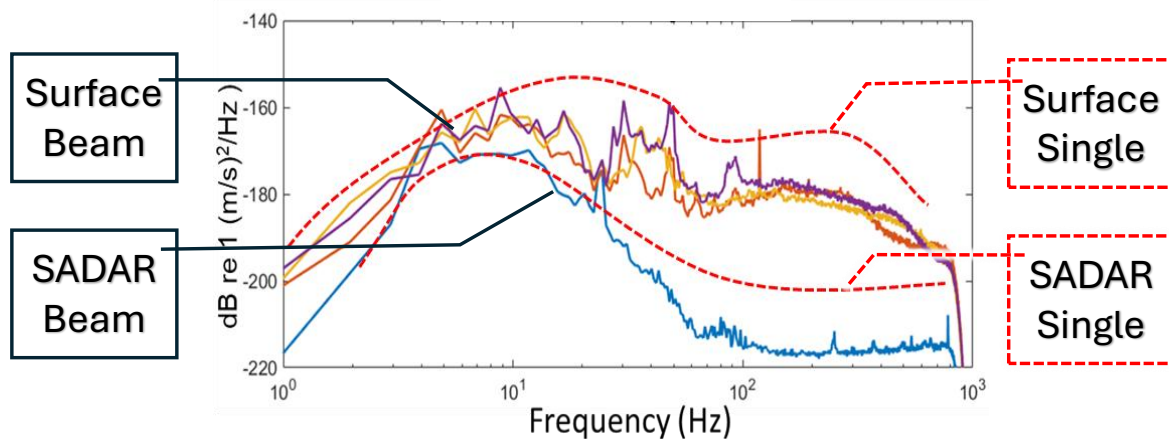


Figure 4. Array gain against ambient noise estimated from A3 (wide-aperture design), compared to the surface array having the same number of elements. The single center geophone at the surface array compared to the SADAR array (at 11 m) at local midday (dashed red lines), and the infinite velocity beam for each array in solid, three plotted for the multicomponent surface array.

A sparse network design as outlined in the Methods section and detailed in Nyffenegger et al. (2023) and Grant et al (2025) usually includes the array performance estimate prior to installation. However, other factors entered the network design because three array designs were being evaluated within the four-array sparse network, and not all required inputs were available to the design team. The overall microseismic monitoring requirements for the BBRS reservoir (~300m depth) posed an optimistic seismic event detection monitoring requirement down to -3 Mw and magnitude of completion goal of  $M_c \approx -2$  Mw for alerting to possible confinement failure within the caprock or the reservoir itself. After a few design iterations and adjusting the arrays as previously stated, the network layout was limited to A1-A4 in the geometry shown in Figure 1 with confidence that the requirements for detection and magnitude of completeness would be met. The shallow depth of the reservoir at the FRS allowed shortened event-to-receiver distances, making these

requirements attainable using a sparse network of only four SADAR arrays and without installing deep instrumented boreholes.

The network performance estimate requires the inputs listed in Nyffenegger et al. (2023) and Grant et al. (2025) to include measurements (noise for example), geophysical models based on measurements (velocity models for example), and parameters required for modeling a source signal level (such as stress drop). The inputs that were not available prior to installation introduced risks primarily mitigated by array and network design. Noise levels and phase velocities were measured in-situ from the SADAR arrays post installation as discussed previously. For example, noise levels were calculated using Welch's method and averaged for each array to generate estimates such as those shown in Figure 4, and stress drop estimates were derived from best fit solutions for moment magnitude based on event spectra. In addition, array gain was estimated from waveforms of located events (after Zhang et al., 2023). The performance prediction is then estimated per array combining the measured and modeled terms for the gridded volume over a magnitude range of -3Mw to -1Mw to determine the minimum source level that results in a detectable signal with SNR of 10 dB for each cell. The 10 dB SNR threshold requirement is chosen from the beamformed waveforms acquired from this network based on automated measurements and quality assessments of the SNR necessary to have confidence in the automated time-of-arrival identification.

As shown in Figure 5, the performance estimates combined for all four arrays determine a minimum locatable magnitude level spatial distribution for the network. The predicted minimum magnitude locatable event does not reach the -3 Mw search minimum across the monitored volume. The performance model predicts the SADAR sparse network is effective down to -2.5 Mw across the active BBRS reservoir at ranges less than 165 m from the injection well. Coverage for either deeper or more shallow geologic strata than the BBRS reservoir and at the extremes of the network is not as complete or uniform for the smallest events, suggesting the effectiveness of the monitoring network approaching the boundary is more like -2.0 Mw.

The automated processing pipeline generates a bulletin containing locations, magnitudes, and attributes that is curated by an analyst for quality assurance. The catalog total population for 47 months of operation is 14,073 events of all quality grades. Many events shallower than 15 m represent surface clutter and currently no unbiased methods exist for this data set to separate known surface clutter detections from shallow valid events. In addition, some events are only detected on 3 arrays with high enough SNR to automatically assign pick times. Filtering out the shallow events ( $z < 15$ ), those with the number of defining arrival times less than four ( $N_{\text{def}} < 4$ ), and quality flags less than (A) results in the 741 high quality events shown in the left most plots of Figure 6. Additional quality analysis is periodically performed on the bulletin (see for example, Hutchenson et al., 2025b). Visual products generated include magnitude and cumulative magnitude frequency distributions for estimating  $M_c$ , total cumulative seismicity, and seismicity/moment as a function of time graphs (not shown here). These plots, configured as

control charts where possible, along with identification of any emerging clusters, represent the daily updates that are potentially available to field operators through SCADA or DCS interfaces.

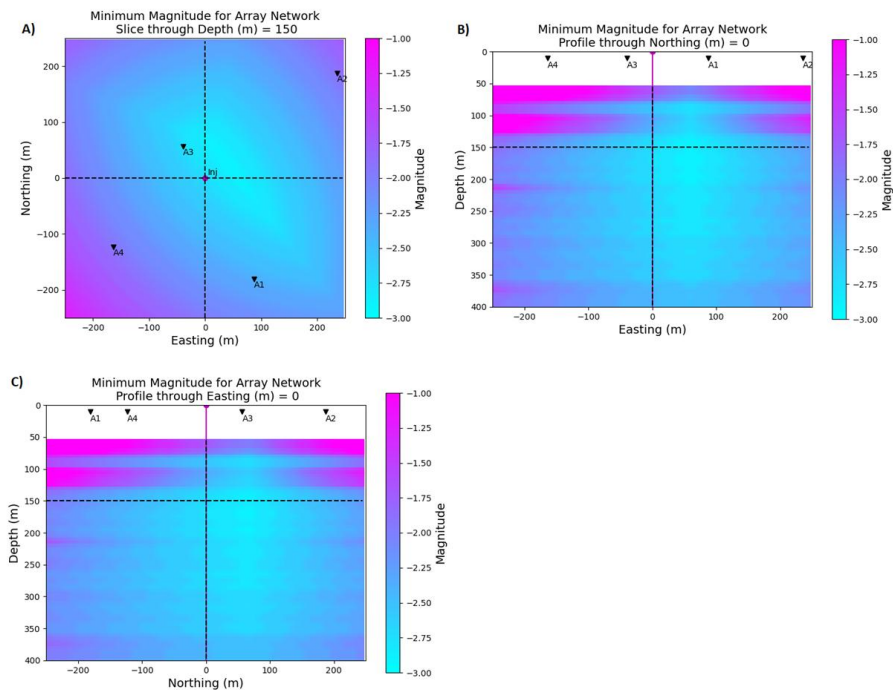


Figure 5. Predicted minimum locatable events (moment magnitude  $M_w$ ) for the monitored volume. For A) horizontal slice through 150m Depth, B) vertical profile through 0m Northing, and C) vertical profile through 0m Easting, the injection well (labelled with a red diamond or labelled "Inj"), and the projection of the locations of the arrays A1-A4 are labeled (after Grant et al., 2025).

Network performance model validation comparing located event spatial distributions to the prediction extends the picture from Grant et al. (2025) with additional data from the analyst reviewed FRS bulletin through the end of 2025. Excluding events with less than 50 m depth and outside of 275 m distance from the injection well, the total number of events considered from the current bulletin is approximately 3486 events of all quality grades. Validation map generation followed Grant et al. (2025): 1) the monitored volume was gridded into 25x25x25m cells, 2) the minimum magnitude event with location inside each bin/cell was recorded, 3) a 3x3x3 smoothing operator was applied over those cells containing information. No effort to quantify statistical significance was performed.

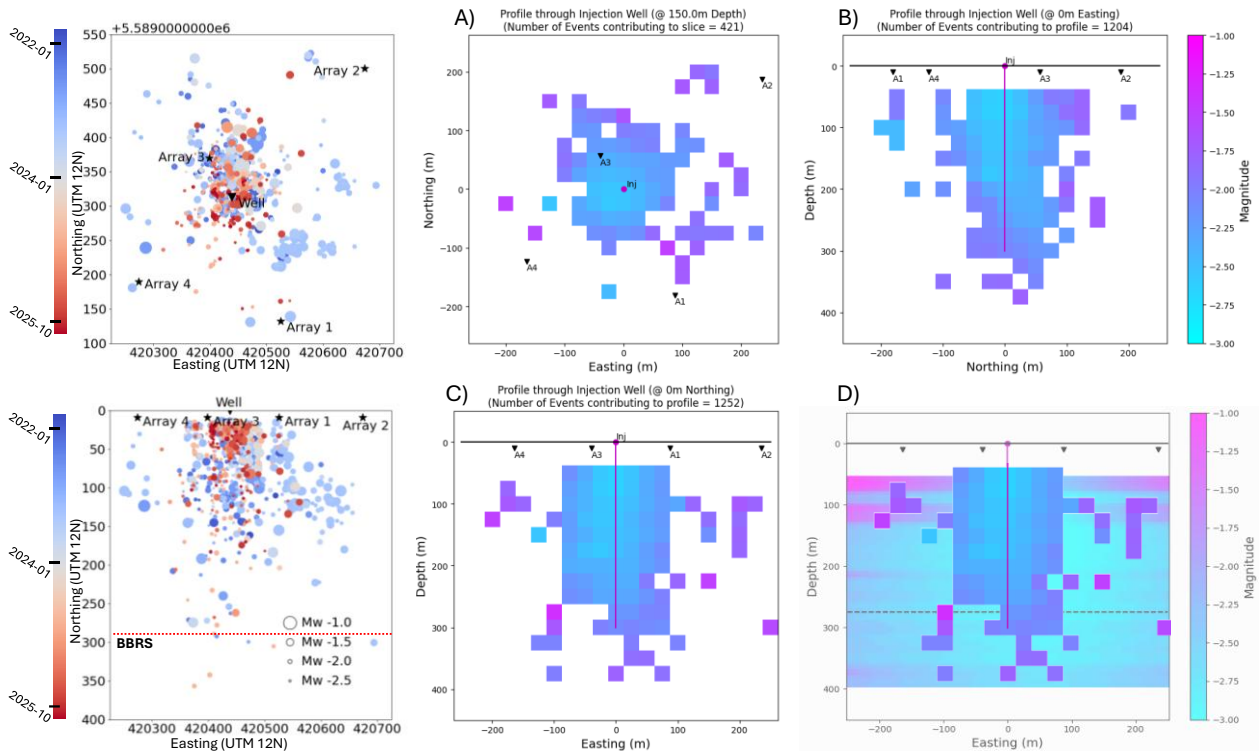


Figure 6. Cross sections through the current validation set. At left: spatial distribution of events map view (upper) and with depth cross section (lower) For 741 events, 4-array location, and  $z > 15$  m. Middle and right show slices at the injection well through A) 150m Depth, B) 0m Northing profile, C) 0m Easting profile, and D) overlay of 0m Easting profile on top of 0m Easting prediction from Figure 5 (mismatched grids).

The estimated minimum observed magnitudes shown Figure 6 middle and right labelled A), B), C), and D), located at the specified slice/cross-section locations ( $\pm 1$  cell) are a measure of fit between the performance model and the observations. The far-left figures display the bulletin results for the time period ending in October 2025, map view (top left) and east-west cross section (bottom left). Mismatch due to location uncertainty, higher-than-modeled noise levels, and non-uniqueness and depth mislocation is expected. The areas in white indicate that there is no validation data support for those cells of the model. The overall agreement using just a visual comparison is good enough to accept the model without changes for the time being considering the low seismicity level at the FRS.

Validation data sets also act to verify the sparse network is operating as expected in terms of detection/location ranges and received signal power. Figure 7 shows the measured received signal power averaged across the array as a function of slant range for 545 reviewed, well-located events occurring over the period November 2021 through October 2025, with depth  $z > 25$  m and distance from the injection well less than 275m. Each event yields one measurement per array for a total of 2180 measurements. Theoretical received signal power versus range curves overlie the plotted data, calculated assuming constant earth model properties and constant stress drop levels, with the only variables being the event magnitude (source level from Grant et al., 2025)

and the range between the source and the receiver arrays. We are in the process of updating and standardizing this analysis in consideration of other SADAR network deployments. Additional important details are included in Grant et al., 2025.

The measured averaged individual channel noise power levels (red dashed line) plotted on top of the data scatter plot and propagation loss estimation in Figure 7, and the approximations for noise levels adjusted for measured gain minimum (~10 dB) and maximum (~18 dB) (green dashed line and dot-dash line respectively), allow a quick data-based estimation of the passive seismic MMV performance. For example, this fused measured event, noise, and model information suggests that for events with  $M_w \leq -2.5$ , reliable detection and high confidence location is limited to a maximum source receiver range of ~450 meters during maximum noise levels (intersection of green dashed line,  $M_w = -2.5$  curve, and supporting data). The analysis using Figure 7 supports a magnitude of completeness  $M_c \approx -2.5$   $M_w$  for the SADAR system bulletin for locatable microseismic events within the network where all SADAR arrays are within 250 meter range from the injection well, but also suggest that  $M_c$  should not be smaller, even considering the short distances.

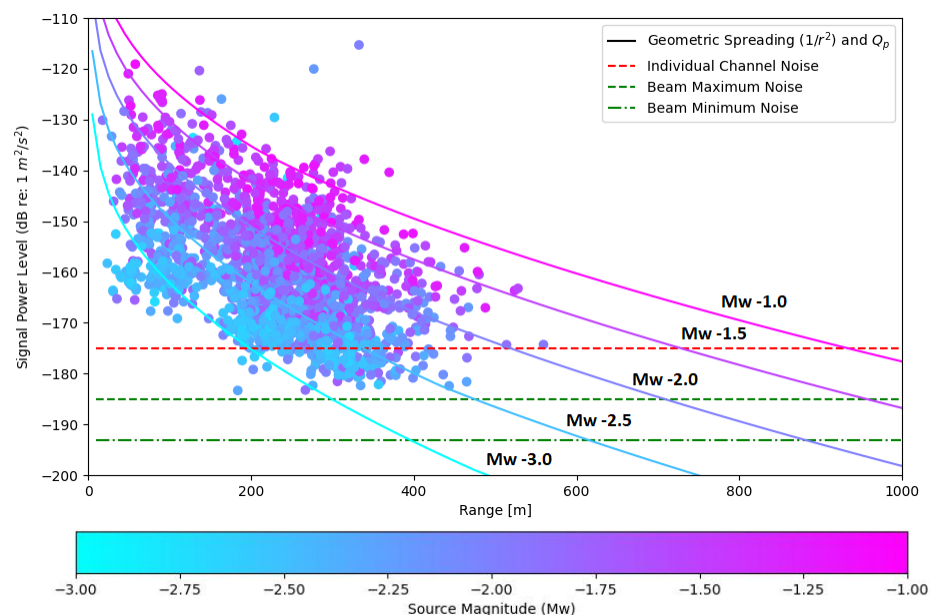


Figure 7. Received peak signal power vs. source-receiver range for 545 well-located events color coded by moment magnitude  $M_w$ . Modeled received signal levels plotted as solid curves include propagation losses. Measured noise RMS estimates are overlain (red dashed line); the low-noise levels are calculated using measured array gains of ~10 dB (green dashed line) and ~18 dB (dot-dash line) applied to the plotted measured noise level.

No active source survey plan that included the SADAR arrays was constructed prior to installation of the arrays. Because the SADAR sparse network was installed after the FRS facility became active, it made no sense to modify the continuing periodic VSP survey plan designed for time-

lapse analysis. In addition, at the time the imaging capability of the SADAR arrays was considered as a proof-of-concept study and was not at an advanced technology readiness level.

The proof-of-concept results, reported in Nyffenegger et al. (2025a, 2025b, 2025c) and Quigley et al. (2025b), confirms that the optimum offset imaging provides a valuable active source imaging functionality for the SADAR array network, summarized in part here. During GHGT-17 field demonstration activities in October 2024, CMC used an Envirovibe source configured with a 16 second 10 Hz - 150 Hz linear sweep to survey the two VSP shot lines shown in Figure 8.

Following the processing sequence outlined in the Methods section, targeted depth points were chosen for  $z=500\text{m}$  in constructing a beam with sufficient width for imaging both the Basal Belly River Sandstone and Manville units. However, the deeper Cambrian units fall on the edge of the beam main lobe and are not expected to show as much improvement in this image. The example targeted beam profiles for A3 shown in Figure 9 (right), show the BBRS reservoir clearly visible at  $\sim 0.25\text{ s}$ , with the Lower Mannville Group reflectors ( $0.85\text{ s}$ ) resolved over a greater offset extent than the BBRS unit. The targeted beamformed image is much improved from a surface sensor receiver gather (Figure 9 left). Targeted beamforming suppresses ground roll and increases the extent of the optimum offset window, improving the vertical definition and horizontal continuity.

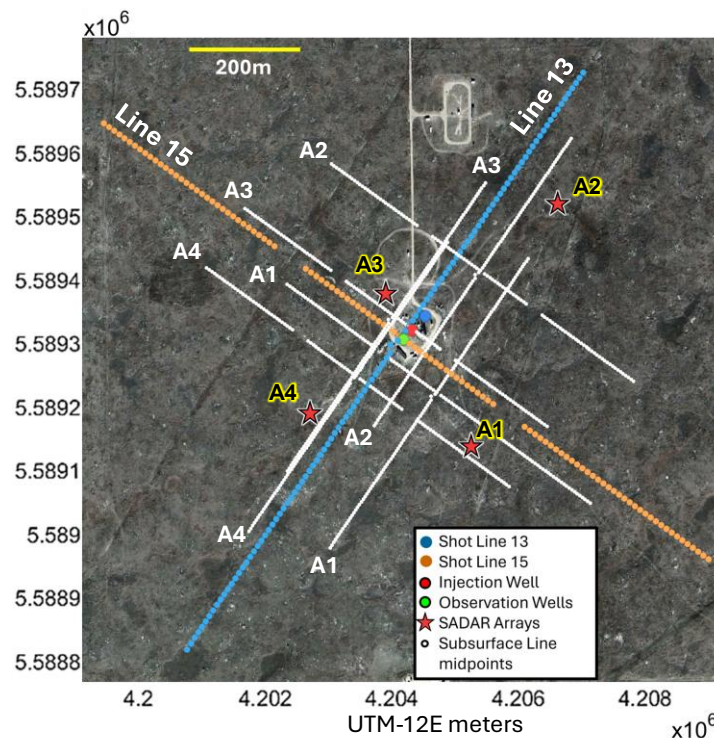


Figure 8. Map of SADAR arrays and VSP survey lines shot in October 2024. Sadar arrays are plotted as red stars, injection well is the red dot near the center, and monitor survey lines 13 and 15 are shown in blue and orange respectively. Midpoint locations are plotted in in white and labeled per array.

Furthermore, the line 15 image (Figure 10, left) demonstrates that offsetting the VSP line from the array benefits the image in an optimum-offset sense by shifting the noise cone to later times in the image, providing a more continuous image of the BBRs. Additionally, example targeted beam profiles for Figure 10 both lines 13 and 15 show the active BBRs injection reservoir clearly visible in the images at approximately 0.25 seconds. The reflectors associated with the Lower Mannville Group (0.85 seconds) are also clearly resolved over a greater extent than the BBRs unit. Lastly, resolution of the Basal Cambrian unit, ~1.2 seconds, 1800 m -2000 m (Burwash et al., 1994) is less improved as expected; beamforming targeted to that horizon provides a better result. The random noise, and air wave and ground roll signal arriving outside the array beam main-response-axis primary lobe are suppressed. However, the effect is not complete at least without applying more sophisticated beamforming to isolate the specular reflections.

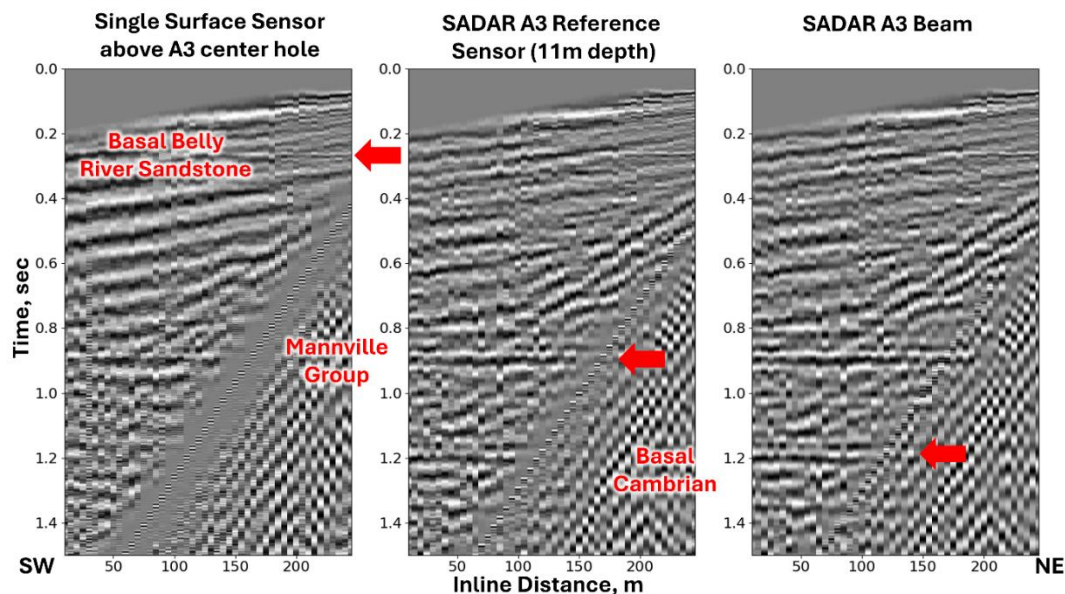


Figure 9. Array 3 subsurface line common receiver gathers from the October 2024 survey, Line 13. A single surface sensor located above the center hole of array A3 is at left, the center-hole, middle-layer reference sensor is shown at center, and the targeted beam profile at right. This image displays results for about half of the line in Figure 8 from the southwest corner, cutting off the surface wave noise cone.

The permanent SADAR network records 2-3 surveys per year at the FRS, but the recurrent surveys do not always repeat the same full suite of shot lines and offsets but rather rotate among a set of lines. In October 2024 during the GHGT-17 demonstration, Line 15 was extended to the northwest and southeast for the first time. For generating images that are stable from survey to survey and suitable for automating time-lapse analysis, surveys will require tight control of shot points, source levels, and source sweep definitions. The output from the source monitor will need to meet the interface control definition of the processing system. The imaging function of the SADAR sparse network is now considered to be beyond proof-of-concept and in active

engineering; the time-lapse analysis of the optimum offset images from standard survey lines is still in a proof-of-concept phase.

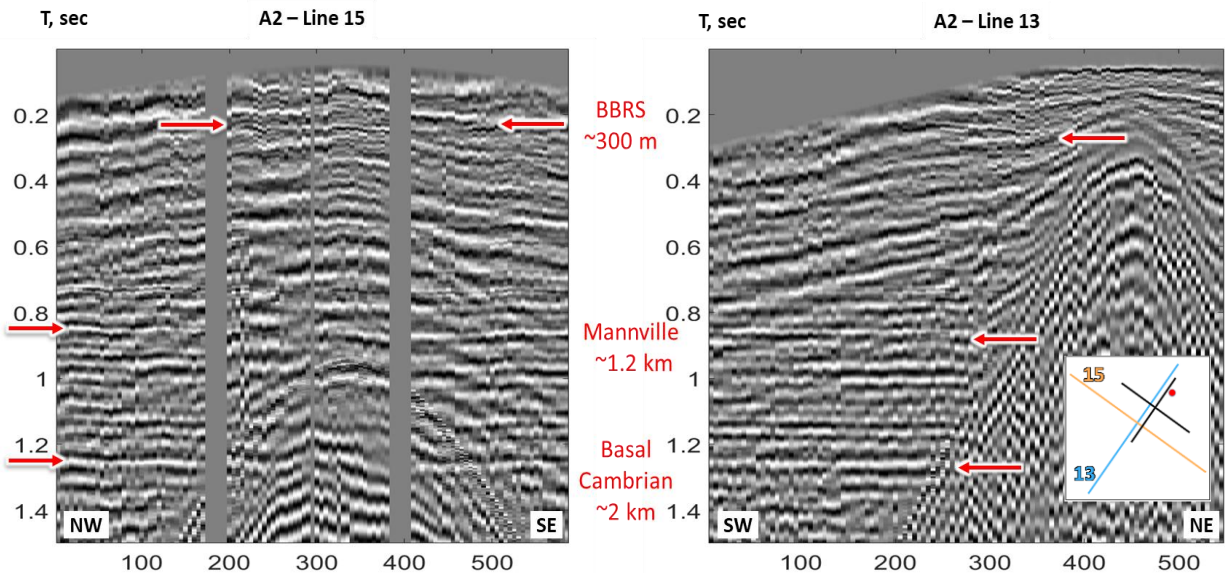


Figure 10. Example targeted beam profile for A2 from the October 2024 survey. The images from line 15 is shown at left and line 13 on the right. Offset along the midpoint line is shown on the x axis. Gaps are no-data zones due to pipelines. The inset on the line 13 image illustrates overall geometries with reflection points plotted as the black lines and the array location as the red dot.

An alternative approach to extending survey lines and surveys repeated on a quarterly basis is to use permanent sources as introduced above in the Methods section (Lawton et al., 2022, Kolkman-Quinn, 2024; Kolkman-Quinn et al., 2025a). Small remotely operated sources mounted on pedestals located as shown in Figure 11 (right, map view) sample the reservoir and geologic stack via specular reflection and optimum offset geometry with the SADAR arrays providing the receivers. The specular reflection arriving after the direct and refracted arrivals but before the ground roll and air blast provides an ideal but single trace sample after beamforming.

Figure 11 center panel shows test signals shot from an Evirovibe unit at SP1 (shown in Figure 11, right panel) received by the SADAR arrays, post correlation. Although difficult to see in the figure, the signal levels at A4 and A3 indicate a clean image of the BBRS reservoir. The BBRS reflection is difficult to see at A1, and of course not expected and absent from A2. The pedestals in Figure 11 are installed at the FRS and testing on newer versions and models of permanent sources is starting.

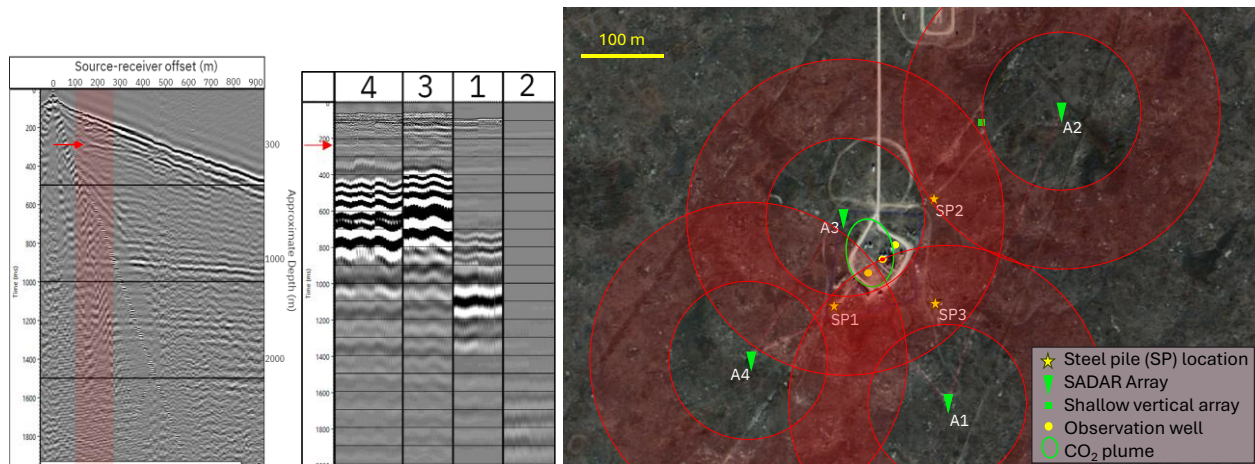


Figure 11. Permanent source optimum offset sampling of the BBRs reservoir. Left panel shows an optimum offset range for the BBRs on a standard VSP survey highlighted in red; center panel shows a correlated conventional vibroseis sweep taken from testing at SP1 shooting into SADAR arrays A1-A4; and right panel map view of the FRS highlights three steel pile location for small automated sources SP1, SP2, and SP3 and shows the four SADAR arrays with optimum offset zones in red. The small red arrows on the left and center panel mark the BBRs reservoir (after the presentation of Nyffenegger et al., 2025c).

## Discussion

The FRS SADAR sparse network systems demonstrate supplying both seismic passive monitoring and active source survey MMV functionality from one set of measurement instrumentation for GCS applications. The individual seismic monitoring functions both using the SADAR sparse network are beyond a proof-of-concept phase and sufficiently developed to address joint or total systems engineering. How best to engineer the combined system to provide the maximum-return-on-investment is an ongoing effort.

The information and processing elements of the joint capability demand a comprehensive systems-engineering approach to ensure that hardware, processing, and information systems operate as an integrated whole. The Methods section presents example approaches from a total system engineering perspective for jointly planning an integrated seismic MMV functionality using sparse networks of SADAR arrays. Typical systems engineering management and technical processes can be applied for producing the integrated seismic MMV functionality, including defining the joint capabilities, deriving the joint requirements, identifying and managing risks, , and lastly evaluation of the joint product as part of the test and evaluation master plan, among the many recognized processes. Moreover, an approach enables seamless alignment with facility operations monitoring and ensures reliable interoperability with DCS and SCADA platforms, supporting consistent data flow, coordinated control functions, and resilient operational performance.

The first steps in total system engineering for combined seismic MMV functionalities were only partly applied in the deployment of the FRS sparse network of SADAR arrays for the passive

seismic monitoring functions. Where the methods were applied, technical and financial value was provided, especially in execution of the system installation. Where the methods could not be applied, deficiencies in the installed systems or operations were observed, but not to the extent to cause the system to fail to meet requirements due to the accepted risks being mitigated by engineering changes prior to deployment. The performance prediction model as well as a data-driven periodically updated performance model validation are critical systems engineering tools for both planning and evaluation.

The evaluation of the arrays and network based on collected data is the process that verifies that the system meets the design requirements under operational conditions. Evaluations are compared to performance predictions (for example Figure 5) and should be designed into the test and evaluation master plan for ensuring that the passive seismic MMV systems meet and continue to meet regulatory and operational requirements as the reservoir changes. The evaluation framework may include a variety of test points, but must include end-to-end evaluations, and should be integrated into the master plan and schedule. For many cases though, an ultimate systems operational evaluation will end up as an ongoing performance assessment because seismicity is not easily controlled and separated into “test events.”

The evaluation should include a variety of metrics including those derived using relationships illustrated in Figure 4, Figure 6, and Figure 7. For example, evaluation of the array design shown in Figure 4, underscores the importance of designing the phased array using measured information, and performing initial site surveys to obtain the information, to mitigate possible performance risks from a design that otherwise would not meet expectations. This is a critical lesson learned from this proving ground deployment in terms of maximizing the return on technology and seismic information, versus accepting risks. Performance metrics based on the seismic survey function have not been addressed.

Such performance analyses built on a database containing the bulletin as well as a suite of other measurements extracted from the waveforms and network, reduced to information, may be automatically presented to facility operators periodically, compared to historical data (e.g., control charts), cast as a moving average summary updated weekly, or computed at operator demand, for highlight changes in the monitoring network or the monitored volume. Therefore, at least some of the performance evaluation information is the same as required for operators to monitor the status of the underground assets, i.e. the geophysical state.

The outcome of the example engineering process for the microseismic MMV function at the FRS is a system that meets requirements, has demonstrated excellent and predictable performance over the 4 years since installation, requires minimal maintenance, admirable systems availability, and unexpected value through additional capabilities. Namely, the passive monitoring system has delivered active source survey imaging capabilities that provide innovative improvements compared to standard borehole and receiver gather images.

Ideally, for using a total systems engineering approach for the seismic MMV functions, the sparse network plan would have included a modeling and modification phase for active source surveys. The CMC-FRS example provides evidence of the value of the imaging capability, demonstrating a usable image where both the random noise and coherent noise arriving outside the array beam main-response-axis primary lobe are suppressed. In comparison though, offsetting the survey line as shown for line 15 Figure 10-left completely avoids the noise cone for the BBRS reservoir (but not the Mannville). A total system plan would have shifted the array location or the survey geometries to provide the optimum offset images required from the start.

The permanent source approach, from a total systems engineering standpoint, has the potential of greatly reducing technical risks while containing costs. The technical capability of the permanent source approach coupled with the permanent arrays will provide time-lapse model conformance verification of changes in the geophysical properties of the reservoir as the plume advances. Cost containment is primarily from providing an active source seismic MMV function that is of known scope, limited complexity for materials, installation, and operations, and amenable to automation from the outset. The operational financial benefits include eliminating repeated mobilization costs and enabling a transition to a condition-based maintenance paradigm, which can be allocated to operating rather than capital expenses.

The SADAR network at the CMC-FRS illustrates that both passive monitoring and active source survey seismic functions can be fused using SADAR compact volumetric phased arrays that require only small footprints. The integrated seismic monitoring capabilities of the SADAR array sparse network will provide facility engineers with improved information for understanding of the physical state of geologic assets. The dual use of the passive monitoring infrastructure can therefore provide warning of containment and conformance anomalies using a spatially sparse sampling of the subsurface, acting as a trigger for conventional expensive 3D surveys.

Nonetheless, some potential capabilities remain in a lower TRL stage. In coming months integration of the permanent remotely operated seismic sources being trialed at the CMC FRS will begin. Application of more advanced beamforming algorithms continues for both seismic monitoring functions, along with processing pipeline development (for active source imaging) and regression testing (for the existing microseismic processing pipeline). Although the resolution and continuity of the structures in the targeted beam image have demonstrated the advantage of phased array beamforming for producing useful, stable, repeatable optimum offset imaging, the time-lapse analysis for quantifying geophysical changes is still under development.

As a last item for discussion, integrated passive monitoring and active survey seismic information for MMV from a single measurement system is a foundational step in developing sparse multiphysics MMV networks. The integrated seismic system provides a common foundation for including other compatible technologies into multiphysics monitoring nodes. Including permanent remote operated seismic sources, the integrated source or receiver “nodes” can form the backbone for supplying power, communications, and potentially limited computation infrastructure

for compatible physical and potentially chemical sensor monitoring technologies. Furthermore, the integrated seismic monitoring capabilities will provide facility engineers with improved information for understanding of the physical state of geologic assets applicable to mining, geothermal, SAG-D and EOR production, gas storage, and waste sequestration projects. Total systems engineering will ensure the architecture is robust, verifiable, and maintainable. And multiphysics nodes will provide the scalable sensing backplane that ties the entire MMV system together.

## Acknowledgements

Research and operations at the Field Research Station are supported by the CMC-CaMI Joint Industry Project members. The authors also acknowledge financial support from Emission Reduction Alberta (ERA) through the Advanced Multi-Physics Sparse Monitoring (AMPS) project. ERA receives its funding from the Government of Alberta through the Technology Innovation Emissions Reduction (TIER) Fund.

## References

- Burwash, R.A., C.R. McGregor, and J. Wilson, 1994, Ch. 5, Precambrian basement beneath the Western Canada Sedimentary Basin: in Geological Atlas of the Western Canada Sedimentary Basin, G.D. Mossop and I. Shetsen (comp.), Canadian Society of Petroleum Geologists and Alberta Research Council, <https://ags.aer.ca/atlas-the-western-canada-sedimentary-basin/chapter-5-Precambrian-basement>
- Douglas, A., 2013, Forensic Seismology and Nuclear Test Bans, Cambridge University Press, Cambridge.
- Grant, E. B., P. A. Nyffenegger, and K. D. Hutchenson, 2025, Predicting and evaluating the performance of sparse permanent array networks for microseismic monitoring. Geoconvention 2025, Calgary Alberta, May 12-14, Available from <https://geoconvention.com/wp-content/uploads/abstracts/2025/114858-predicting-and-evaluating-the-performanc>
- Hunter, J.A., and S.E. Pullan, 1989, The optimum offset shallow seismic reflection technique. Proceedings of the Symposium on the Application of Geophysics to Engineering and Environmental Problems, EEGS, 143-174.
- Hutchenson, K.D., J. Jennings, E.B. Grant, D. Quigley, J. Yelton, and P.A. Nyffenegger, 2025a, Persistent microseismic monitoring using robust permanent SADAR arrays. Proceedings of the *Carbon Capture, Utilization, and Storage Conference and Exhibition, 3–5 March 2025. Carbon Capture, Utilization, and Storage Conference and Exhibition, 3–5 March 2025.* (pp. pp. 198-203). <https://doi.org/10.15530/ccus-2025-4184595>
- Hutchenson, K.D., D. Quigley, J. Yelton, E.B. Grant, and P.A. Nyffenegger, 2025b, Capabilities of microseismic monitoring using robust permanent SADAR arrays. Proceedings of the Fifth International Meeting for Applied Geoscience & Energy. Fifth International Meeting for Applied Geoscience & Energy, 25-28 August, 2025, Houston.
- Kolkman-Quinn, B., D. Lawton, J. Cooper, and M. Macquet, 2025a, Onshore sparse seismic monitoring design scenario using permanent sources and receivers. 86th EAGE Annual Conference & Exhibition, Jun 2025, Volume 2025, 1 – 5. DOI: <https://doi.org/10.3997/2214-4609.2025101370>
- Kolkman-Quinn, B., D. Lawton, M. Macquet, J. Cooper, 2025a, Permanent sparse monitoring design concepts for CO<sub>2</sub> plume monitoring, Geoconvention 2025, Calgary Alberta, May 12-14, Available from: <https://geoconvention.com/wp-content/uploads/abstracts/2025/114499-permanent-sparse-monitoring-design-conce>
- Kolkman-Quinn, B., D. Lawton, M. Macquet, K. Osadetz, H. Behmanesh, J. Cooper, and N. Wildgust 2025b, Analysis of technical challenges for large-scale geological carbon storage: A western Canadian perspective. 86th EAGE Annual Conference & Exhibition, Jun 2025, Volume 2025. DOI: <https://doi.org/10.3997/2214-4609.2025101354>

Kolkman-Quinn, B., D. Lawton, and M. Bertram, and M. Macquet, 2024, Sparse Seismic Monitoring of Geologic Carbon Storage. Proceedings of the 17th Greenhouse Gas Control Technologies Conference (GHGT-17) 20-24 October 2024, Available at SSRN: <https://ssrn.com/abstract=5068174> or <http://dx.doi.org/10.2139/ssrn.5068174>

Lawton, D.C., Dongas, J., Osadetz, K., Saeedfar, A., and Macquet, M., 2019, Chapter 16: Development and analysis of a geostatic model for shallow CO<sub>2</sub> injection at the Field Research Station, Southern Alberta, Canada. in T. Davis, M. Landro, and M. Wilson, eds., *Geophysics and Geosequestration*: Cambridge University Press, 280-296, <https://doi.org/10.1017/9781316480724.017>.

Lawton, D., Hunter, T., Kolkman-Quinn, B., Monsegny, J., Bertram, M., Maidment, G., 2022, Sparse Optimum-offset Seismic Surveys for Monitoring Gigatonne-scale CCS Projects, presented at the SEG workshop:- Toward Gigatonnes CO<sub>2</sub> Storage — Grand Geophysical Challenge; 26-30 June 2022, Stanford, CA.

Nyffenegger, P.A., E.B Grant, J. Zhang, J. Jennings, D. Quigley, K.D. Hutchenson, M.A. Tinker, M. Macquet, and D.C. Lawton, 2023a, Estimates of performance model factors for passive microseismic SADAR phased arrays at the Newell County Facility: Presented at GeoConvention 2023, Calgary, Available from: <https://geoconvention.com/wp-content/uploads/abstracts/2023/91418-estimates-of-performance-model-fac.pdf>

Nyffenegger, P.A., K.D. Hutchenson, D. Quigley, J. Yelton, M. Dahl, 2025a, Integrated passive and active source sparse seismic monitoring for geologic carbon storage projects. Proceedings of the Fifth International Meeting for Applied Geoscience & Energy. Fifth International Meeting for Applied Geoscience & Energy, 25-28 August, 2025a, Houston.

Nyffenegger, P.A., D.C. Lawton, M. Macquet, D. Quigley, B. Kolkman-Quinn, and K.D. Hutchenson, 2025b, Advances in coupled passive and active seismic monitoring for large-scale geologic carbon storage projects, in Wilson, M., T. Davis, and M. Landro, eds., *Geophysics and the Energy Transition*: Elsevier Press, 333-354.

Nyffenegger, P.A., D. Quigley, B. Kolkman-Quinn, J. Yelton, K. D. Hutchenson, E. B. Grant, 2025c, Integrating passive and active seismic monitoring applications in sparse monitoring networks using SADAR arrays, First EAGE Workshop on Geophysical Techniques for Monitoring CO<sub>2</sub> Storage, Oct 2025, Volume 2025, p.1 – 5, DOI: <https://doi.org/10.3997/2214-4609.202585014>

Nyffenegger, P.A., M.A. Tinker, J. Zhang, E.B. Grant, K.D. Hutchenson, and D.C. Lawton, 2022, Compact phased arrays for microseismic monitoring: *First Break*, 40, 4, 69-74. <https://doi.org/10.3997/1365-2397.fb2022033>.

Nyffenegger, P.A., J. Zhang, E.B. Grant, D. Quigley, K.D. Hutchenson, M.A. Tinker, D.C. Lawton, and M. Macquet, 2023b, Performance and outlook for the SADAR array network at the Newell County Facility: *First Break*, 41, 4, 56-62, <https://doi.org/10.3997/1365-2397.fb2023028>

Pevzner, R., R. Isaenkov, S.Yavuz, A. Yurikov, K. Tertyshnikov, P. Shashkin, B. Gurevich, J. Correa, S. Glubokovskikh, T. Wood, B. Freifeld, and P. Barraclough, P., 2021, Seismic monitoring of a small CO<sub>2</sub> injection using a multi-well DAS array: Operations and initial results of stage 3 of the CO<sub>2</sub>CRC Otway Project: *International Journal of Greenhouse Gas Control*, 110, 103437. <https://doi.org/10.1016/j.ijggc.2021.103437>

Quigley, D., P. A. Nyffenegger, K. D. Hutchenson, and J. Yelton, 2025a, Active source sparse imaging using permanent SADAR arrays. Proceedings of the *Carbon Capture, Utilization, and Storage Conference and Exhibition, 3–5 March 2025. Carbon Capture, Utilization, and Storage Conference and Exhibition, 3–5 March 2025*. (pp. pp. 219-223). ASME. <https://doi.org/10.15530/ccus-2025-4186259>

Quigley, D., K.D. Hutchenson, P. A. Nyffenegger, and M. Dahl, 2025b, Active source imaging from Newell County geologic carbon storage facility using a sparse network of SADAR arrays. *Geoconvention 2025*, Calgary Alberta, May 12-14, <https://geoconvention.com/wp-content/uploads/abstracts/2025/114805-active-source-imaging-from-newell-county>

Zhang, J., E. B. Grant, P. A. Nyffenegger, M. Tinker, K. Hutchenson, 2022, Seismic monitoring using compact phased arrays: CO<sub>2</sub> sequestration monitoring. 483-487. <https://doi.org/10.1190/image2022-3751162.1>.

Zhang, J., K.D. Hutchenson, P.A. Nyffenegger, E.B. Grant, J. Jennings, M.A. Tinker, M. Macquet, and D.C. Lawton, 2023, Performance comparison of compact phased arrays and traditional seismic networks for microseismic monitoring at a CO<sub>2</sub> sequestration test site: *The Leading Edge*, 42(5), 332-342. <https://doi.org/10.1190/le42050332.1>